# Mechanistic Insight into the Hydrogenation of Acetylene on the Pd2/g-C3N4 Catalyst: Effect of Pd Clustering on the Barrier Energy and Selectivity

**Sayyed Mahdi Hosseini**
Isfahan University of Technology
**Mehran Ghiaci**
Isfahan University of Technology
**Hossein Farrokhpour** ( farrokhphossein@gmail.com )
Chemistry Department-Isfahan University of Technology

**Research Article**

**Keywords:** Acetylene, Hydrogenation, Pd cluster, g-C3N4, Selectivity, Ethylene

**Posted Date:** March 11th, 2021

**DOI:** https://doi.org/10.21203/rs.3.rs-259183/v1



**Version of Record:** A version of this preprint was published at Structural Chemistry on April 19th, 2021.
See the published version at https://doi.org/10.1007/s11224-021-01781-3.

# Abstract

In this work, the hydrogenation of acetylene on the $Pd_2/g\text{-}C_3N_4$ catalyst is investigated by the Density Functional Theory (DFT) and Quantum Theory of Atoms in Molecules (QTAIM) calculations. The Pre-reactant (R), transition states (TSs), and the intermediates (IMs), involved in the hydrogenation process, are characterized from the point of view of energy and structure. The calculated energy barrier for the hydrogen transfer to the acetylene and ethylene are 6.77 and 12.28 kcal/mol, respectively which shows that the $Pd_2/g\text{-}C_3N_4$ catalyst has good selectivity for the conversion of acetylene to ethylene rather than ethane. Comparing the values of these energy barriers with those of the hydrogenation of acetylene on the $Pd/g\text{-}C_3N_4$ catalyst (21.53 and 38.88 kcal/mol, respectively) shows that the increase in the number of the Pd atoms decreases the energy barriers of the hydrogenation reaction and increases the selectivity of the catalyst for the ethylene production.


# Introduction

Ethylene is an important raw material with wide applications in petrochemical industries [1]. Generally, the production of ethylene is performed via the steam cracking of hydrocarbons. The main disadvantage of this method is the catalyst poisoning leading to the reduction of catalyst lifetime.[2]. So, the catalytic hydrogenation of acetylene followed by the classical Horiuti–Polanyi mechanism has been considered as the best method for ethylene production on large scales [3]. An efficient catalyst for acetylene hydrogenation should have high activity and selectivity for ethylene production [4]. In this regard, the noble transition metals, especially, palladium (Pd)-based catalysts are widely used for this purpose. Because they show good selectivity for ethylene production because of their superior hydrogen solubility and good ability for dissociation of $H_2$ molecules [5,6]. There are several experimental works aiming production of ethylene via acetylene hydrogenation in a selective manner in which the structure of the Pd-based catalyst plays a critical role in achieving a good selectivity [7-12].

Huang et al. prepared the dispersed Pd atoms on the $g\text{-}C_3N_4$ using atomic layer deposition and performed the hydrogenation of acetylene on the $Pd_1/g\text{-}C_3N_4$ catalyst [7]. Boucher et al. performed the hydrogenation of styrene and acetylene on the catalyst composed of the Pd atoms binding to the Cu surface [8]. Panpranot et al. investigated the catalytic efficiency of Pd catalyst supported on nanocrystalline $TiO_2$ ($Pd/TiO_2$) for the selective hydrogenation of acetylene in the presence of excess ethylene [11]. The same group also examined the effect of the phase composition of the $TiO_2$ crystalline support on the physicochemical and catalytic properties of the $Pd/TiO_2$ catalyst on the selective hydrogenation of acetylene [12].

There are several theoretical studies of the clarification of the hydrogenation mechanism of acetylene on the Pd-based catalysts, and the interaction between the different forms of Pd and the substrates [13-16]. Meng et al. studied the hydrogenation of acetylene on the $TiO_2$ supported $Pd_aAg_b$ ($a$+$b$=4) catalyst using the density functional theory (DFT)+U method [13]. The hydrogenation of acetylene using the $Pd_4$ cluster

on the anatase $TiO_2$ (101) support was studied by Yang et al. [14]. Ma et al. performed the DFT study of the selective hydrogenation of acetylene on the P-doped Cu (111) surface [15]. The effect of the size of Pd cluster ($Pd_n$) and its geometry on the hydrogenation of acetylene has been investigated [17-20]. Li et al. investigated the effect of the size of Pd clusters on acetylene hydrogenation in the absence of any support [17]. Pu et al. investigated the effect of $Pd_n$ clusters with different sizes (n=2-8) on acetylene hydrogenation by the DFT calculations. They proposed two pathways for acetylene hydrogenation including (*a*) ethene formation as the main product via vinyl intermediate and (*b*) the vinylidene, ethylidene, and ethylidene as the intermediates participating in the hydrogenation process. Also, They showed that the reaction pathway depends strongly on the size of $Pd_n$ clusters so that for $n<4$, the hydrogenation reaction proceeded through the vinyl intermediate while the other pathway via the vinylidene intermediate was the main pathway for the larger Pd clusters [17].

Due to the high activity of Pd catalysts, the over-hydrogenation of ethylene is always a deep concern. Therefore, designing a selective catalyst for ethylene production to eliminate extra purification steps in its synthesis and prevent ethane production is considered a challenging task in acetylene hydrogenation [21-22]. Various strategies have been so far reported for the promotion of the performance of Pd-based catalysts for the acetylene hydrogenation which one of the important of them is the doping of the Pd cluster with other noble metals such as Au [23], Pb [24,25], Cu [26], Ag [27,28,29], and Ga [30,31]. The other important strategy is using single-atom alloys (SAA) and single-atom catalysts (SAC), immobilized on solid supports such as ZnO [32], fiberglass [33], graphene [34], $Al_2O_3$ [35], and graphitic carbon nitride ($g\text{-}C_3N_4$) [6-7] which has shown interesting results in acetylene hydrogenation. Among the solid supports, $g\text{-}C_3N_4$ is always considered a suitable candidate for the deposition of Pd active sites [36-38]. It has some outstanding features such as low-cost fabrication, short time and easy synthesis, adjustable surface area, good dispersion potential for active sites, and high coordination ability for metal clusters and nanoparticles. Huang et.al showed that Pd single-atom immobilized on the surface of $g\text{-}C_3N_4$ has a better selectivity in acetylene hydrogenation compared to nanoparticle ones [7]. Zhao et al.'s theoretical study aiming to demonstrate the acetylene hydrogenation mechanism over the $Pd_1/g\text{-}C_3N_4$ catalyst showed that the Pd atom tended to adsorb on the top of the sixth fold cavity of $g\text{-}C_3N_4$ as the most accessible site. Moreover, the $Pd_1/g\text{-}C_3N_4$ catalyst showed better selectivity to ethylene production in comparison to ethane production as expected from the experimental studies [39]. Kang et al. investigated the catalytic activity of the $Pd_1/g\text{-}C_3N_4$ catalyst for acetylene hydrogenation by replacing the nitrogen and carbon atoms of $g\text{-}C_3N_4$ with the sulfur atom (S) [40]. It was observed that the $Pd_1/g\text{-}C_3N_4$ containing sulfur-doped carbon atoms have higher activity for the dissociation of $H_2$ molecules while better selectivity is achieved for sulfur-doped nitrogen ones.

To the best of our knowledge, there is no theoretical mechanistic study of acetylene hydrogenation over $Pd_n/g\text{-}C_3N_4$ structures with n>1 in the literature. Our recent theoretical study on the adsorption of small-size $Pd_n$ clusters (n=2, 4, 6, and 8), immobilized on the $g\text{-}C_3N_4$ quantum dot, reveals that the $Pd_2$ cluster has the highest adsorption energy among the other selected Pd clusters [41]. In this work, the DFT

calculations are performed to understand the exact mechanism of acetylene hydrogenation on the $Pd_2$/g-$C_3N_4$ catalyst and see the effect of the added Pd atom on the activity of catalyst compared to that of $Pd_1$/g-$C_3N_4$ catalyst reported in references 39 and 40. Our calculated results show less activation energy for acetylene hydrogenation using the $Pd_2$/g-$C_3N_4$ compared to the $Pd_1$/g-$C_3N_4$ catalyst and better selectivity for ethylene production which is in good accordance with the experimental data in the literature [39,45-47].

### Computational details

The structure of all reactants ($Pd_2$/g-$C_3N_4$, $C_2H_2$, and $H_2$), pre-reactant (R), transition states (TSs), and intermediates (IMs) were optimized in the gas phase using the DFT method employing B3PW91 functional [42]. The 6-311+G(d,p) and Los Alamos effective core pseudo-potential (ECP) (LANL2DZ) basis set were used for the g-$C_3N_4$ and $Pd_2$, respectively. The frequency calculations were performed on all optimized structures to check their correct positions on their potential energy surfaces in the hydrogenation pathway and determine their electronic energies, enthalpies, Gibbs free energies, and zero-point energies. The suitability of the selected DFT functional and basis set for the considered systems have been investigated by Zhao et al [39]. The intrinsic reaction coordinate (IRC) calculations were performed to make sure that each TS structure was related to its corresponding reactants and products in the reaction mechanism. The highest occupied molecular orbital (HOMO) and lowest unoccupied molecular orbital (LUMO) of the structures were calculated to obtain the bandgap energies and donor-acceptor properties of structures. The Quantum Theory of Atoms in Molecules (QTAIM) calculations were performed using Multiwfn 3.4 software [43] for better structural characterization of the TSs and confirming the proposed mechanism of the reaction. All DFT calculations were performed using the Gaussian 09 Quantum Chemistry Package [44].

## Results And Discussion

### The optimized structure of the $Pd_2$/g-$C_3N_4$ catalyst and its charge distribution

A quantum dot of g-$C_3N_4$ is selected as a model of substrate for the deposition of the $Pd_2$ cluster. The g-$C_3N_4$ has two main structural forms based on the s-triazine and tri-s-triazine building blocks so that the latter form is always considered as the most stable form of g-$C_3N_4$ [39-41]. A layer of g-$C_3N_4$ composed of three tri-s-triazine units was selected and optimized (see Figure 1). The nitrogen atoms in this model are classified into two classes: (*a*) saturated nitrogen atoms which are bonded to three carbon atoms (N1) and (*b*) pyridine-like nitrogen atoms which are bonded to two carbon atoms and are located at the corners of the sixth fold cavity (N2). Since 2p orbitals of N2 atoms have the main contribution in the valance band of g-$C_3N_4$, their lone pairs electrons have the main role in the chemical activity of g-$C_3N_4$ compared to the N1 atoms [41]. On the other hand, 2p orbitals of the N1 and C atoms orbitals have a major contribution to the conduction band of g-$C_3N_4$ [41].

The $Pd_2$ cluster is optimized, separately and placed on the top of the sixth fold cavity of g-$C_3N_4$ aiming to achieve the maximum interaction with the lone pairs of N2 atoms. The comparison of the structure of g-$C_3N_4$ in the $Pd_2$/g-$C_3N_4$ complex with the optimized structure of isolated g-$C_3N_4$ shows that the presence of the $Pd_2$ creates more wrinkles and waves in the structure of g-$C_3N_4$ (Figure 1). The bond length of the $Pd_2$ cluster in the optimized structure of the $Pd_2$/g-$C_3N_4$ is 2.74 Å which shows the elongation of the Pd-Pd bond length compared to the isolated $Pd_2$ cluster due to the strong interaction between the Pd atom, directed to the support, and the carbon atom of one of the tri-s-triazine units. The calculated partial atomic charges of these Pd and C atoms in the $Pd_2$/g-$C_3N_4$ is 0.37e and -1.458e, respectively. Comparison of the charge of this C atom in the complex with that in the isolated g-$C_3N_4$ (0.297e) shows a strong charge transfer from the $Pd_2$ to g-$C_3N_4$ confirming a strong interaction between the Pd and carbon atom (see Figure 2). The angle between the $Pd_2$ axis and the g-$C_3N_4$ plane is 46.0°.

## HOMO and LUMO of reactants

Table 1 reports the energies of the HOMO and LUMO of $C_2H_2$, $H_2$, g-$C_3N_4$, $Pd_2$/g-$C_3N_4$, and $C_2H_2$.$Pd_2$/g-$C_3N_4$ structures along with their energy gaps. The shapes of the HOMO and LUMO of g-$C_3N_4$, $Pd_2$/g-$C_3N_4$, and $C_2H_2$.$Pd_2$/g-$C_3N_4$ structures have been shown in Figure 3. According to our previous work [41], immobilization of the $Pd_2$ cluster on the surface of g-$C_3N_4$ causes the decrease of the energy gap of the $Pd_2$/g-$C_3N_4$ complex compared to the isolated g-$C_3N_4$ because of creating new electronic states between the HOMO and LUMO of g-$C_3N_4$ [41]. These new electronic states cause the increase of the photocatalytic activity of the $Pd_2$/g-$C_3N_4$ complex compared to the bare g-$C_3N_4$. Comparison of the difference between the energy of the HOMO of $Pd_2$/g-$C_3N_4$ and that of LUMO of $C_2H_2$ (-4.25 eV) with the energy difference between the HOMO of $C_2H_2$ and LUMO of $Pd_2$/g-$C_3N_4$ (-5.24 eV) shows that the $C_2H_2$ is an electron acceptor species. A similar comparison between the $Pd_2$/g-$C_3N_4$ and $H_2$ shows that the $H_2$ is also an electron acceptor. The smaller value of the energy difference between the HOMO of $C_2H_2$ and LUMO of $Pd_2$/g-$C_3N_4$ compared to the corresponding value for the $H_2$ and $Pd_2$/g-$C_3N_4$ indicates the better adsorption of the $C_2H_2$ on the $Pd_2$/g-$C_3N_4$ compared to the $H_2$ molecule.

## Adsorption of $H_2$ and $C_2H_2$ on $Pd_2$/g-$C_3N_4$

Essentially for a heterogeneous catalyst containing the Pd cluster, it is important to use the maximum active site of the cluster after immobilization. Therefore, it is necessary to find the most stable site for the adsorption of $H_2$ and $C_2H_2$ molecules on the surface of the $Pd_2$/g-$C_3N_4$ catalyst. For this purpose, the $H_2$ molecule approaches the catalyst in the dissociated and bonded forms, separately (see Figures S1(a) and (b)). As seen in Figure S1(a), the $H_2$ molecule is located near one Pd atom which is farther from the surface of g-$C_3N_4$. In Figure S1(b), it is assumed that the $H_2$ molecule has been dissociated on the $Pd_2$/g-$C_3N_4$ catalyst and each of its H atoms is interacting with one of the Pd atoms. The two initial structures lead to the same structure after the optimization so that the two hydrogen atoms of the $H_2$ molecule is interacting with one Pd atom ($H_2$.$Pd_2$/g-$C_3N_4$; see Figure S1(c)). The reason for the interaction of the $H_2$

molecule with this Pd atom could be attributed to its negative Mulliken charge which provides a good potential for the participation in electron donation to reactants.

In the next step, the $C_2H_2$ is approached to the $H_2.Pd_2/g\text{-}C_3N_4$ complex to form the pre-reactant ($C_2H_2.H_2/g\text{-}C_3N_4$) for the start of the reaction. Figure S2 shows two proposed structures for the pre-reactant (R1 and R2). The best selected initial orientation of the $C_2H_2$ relative to the $Pd_2$ in the $C_2H_2.H_2.Pd_2/g\text{-}C_3N_4$ complex is such that its molecular axis is in a vertical position relative to the axis of the $Pd_2$ (R1 in Figure S2). In this case, the simultaneous interaction of each C atom of $C_2H_2$ with both Pd atoms is possible. It will be shown that the interaction of the C atoms of $C_2H_2$ with the Pd atom, located far away from the surface of $g\text{-}C_3N_4$, is stronger than the interaction with the other Pd atom. As previously shown in Figure 2b, the Pd atom located further away from the $g\text{-}C_3N_4$ has a more negative Mulliken charge compared to the other Pd atom. Therefore, this Pd atom has good potential for electron donation to the reactants ($H_2$ and $C_2H_2$). Therefore, the $C_2H_2$ and $H_2$ interact mainly with the upper Pd atom in the optimized structure of $C_2H_2.H_2.Pd_2/g\text{-}C_3N_4$ complex. Due to the adsorption, the H-H bond length increases to 0.93 Å compared to that of an isolated $H_2$ molecule (0.74 Å). Moreover, the increase of the C≡C bond length is seen for the acetylene in the $C_2H_2.H_2.Pd_2/g\text{-}C_3N_4$ complex (1.28 Å) compared to isolated acetylene molecule (1.19 Å). These observations confirm the activation of the $H_2$ and $C_2H_2$ molecules by the catalyst and indicate that the initial complex (R1 in Figure S2) is suitable for starting the hydrogenation process. Considering the adsorption energies of reactants, it can be concluded that the adsorption of acetylene on the catalyst (-28.84 kcal/mol) is stronger than that of the $H_2$ molecule (-13.23 kcal/mol) which is in agreement with the frontier molecular orbital analysis performed in the previous section.

The energy difference between the HOMO of $C_2H_2.Pd_2/g\text{-}C_3N_4$ and the LUMO of $H_2$ (-5.93 eV) is smaller than the energy difference between the HOMO of $H_2$ and the LUMO of $C_2H_2.Pd_2/g\text{-}C_3N_4$ (-9.07 eV). This shows a charge transfer from the HOMO of $C_2H_2$ .$Pd_2/g\text{-}C_3N_4$ complex to the LUMO of $H_2$ molecule and leads to a strong interaction between these reactants and can better describe the co-adsorption configuration of the $H_2.C_2H_2.Pd_2/g\text{-}C_3N_4$ complex.The calculated co-adsorption energy of the $H_2.C_2H_2.Pd_2/g\text{-}C_3N_4$ complex is -45.3 kcal/mol which is greater than the value related to the adsorption of isolated $C_2H_2$ (-28.84 kcal/mol) and $H_2$ (-13.23 kcal/mol) molecules on the $Pd_2/g\text{-}C_3N_4$ catalyst. Eq. (1) is used for the calculation of the co-adsorption energy of $H_2.C_2H_2.Pd_2/g\text{-}C_3N_4$ complex.

$$E_{co-adsorption} = E_{complex} - E_{catalyst} - E_{H_2} - E_{acetylene} \quad (1)$$

where $E_{complex}$ is the electronic energy of $H_2.C_2H_2.Pd_2/g\text{-}C_3N_4$ complex. The $E_{acetylene}$, $E_{catalyst}$, and $E_{H2}$ are the electronic energies of isolated optimized acetylene, $Pd_2/g\text{-}C_3N_4$, and $H_2$ molecule, respectively

**Mechanism of acetylene hydrogenation on the $Pd_2/g\text{-}C_3N_4$ catalyst**

As previously mentioned, two initial structures, R1 and R2 (Figure S2), were considered as the starting structures for the hydrogenation mechanism. Zhao et al. demonstrated that the hydrogenation pathway via the R1 complex in the presence of $Pd_1/g\text{-}C_3N_4$ single-atom catalyst requires less activation energy compared to the R2 ones [39]. Also, they reported that the hydrogenation pathway via the R1 complex had more selectivity to the ethylene production rather than ethane production [39]. Therefore, the R1 structure is selected as the initial structure for the hydrogenation mechanism on the $Pd_2/g\text{-}C_3N_4$ catalyst.

Considering the R1 as a starting complex, two consecutive pathways are proposed for the hydrogenation mechanism. In the first pathway, the acetylene is converted to ethylene (IM3) via the three transition states (TS1, TS2, and TS3) (see Figure 4). In the second pathway, ethylene (IM3) is hydrogenated more and converted to ethane (P) via two transition states (TS4 and TS5). To obtain the activation energy of each step, the $E_{\text{co-adsorption}}$ of each complex involve in each step is calculated using Eq. (1). The energy difference between the $E_{\text{co-adsorption}}$ of the reactant and TS of each step is considered as the activation energy (Figure 4). Figures 5-9 show the optimized structures of the complexes (R1, IMs, and TSs) involved in the pathways shown in Figure 4. Also, the important interaction paths for each complex, obtained from the QTAIM calculations, are shown in the Figures. The position of the bond critical points (BCPs) (dots) and their calculated electron density ($r$) have been identified in the Figures.

***R1® TS1® IM1.*** The calculated value of the activation energy for the conversion of the R1 complex to IM1 via TS1 is 6.77 kcal/mol (see Figure 5). The optimized structure of TS1 is similar to the R1 complex except that the $H_2$ bond length increases to 2.77 Å in the structure of TS1 indicating the complete dissociation of the $H_2$ molecule on the catalyst. The calculated vibrational mode of TS1 with the imaginary vibrational frequency (n=-470$i$ $cm^{-1}$) is shown in Figure S3. The direction of the displacement vector of one of the H atoms of the dissociated $H_2$ molecule is towards the C atom of the acetylene indicating the H transfer from the Pd to C atom. Comparison of the arrangement of the BCPs in the R1 complex with that of TS1 shows that the BCP No.1 (BCP1; $r$=0.1732 a.u), related to the interaction path between two H atoms of $H_2$ molecule in the R1 complex, disappears. Also, a new BCP (BCP4) is formed between one of the H atoms of the $H_2$ molecule and the C atom of acetylene in the TS1 complex. As seen, this H atom has simultaneous interaction with the Pd and C atoms via the interaction paths related to the BCP2 ($r$=0.1189 a.u) and BCP4 (($r$=0.1444 a.u) in the structure of TS1. Due to the interaction of this H atom with the C atom of acetylene, the C-H bond length increases from 1.08 Å in the R1 complex to 1.43 Å in the IM1 complex. These observations confirm the transfer of the H atom from the Pd site to the C atom of acetylene for the formation of the vinyl compound. It is important to note that there is no BCP between two Pd atoms in the structure of the complexes shown in Figure 5 and each Pd atom is interacting with the C atoms of acetylene independent of the other one. In the R1 complex, each of the Pd atoms is interacting with one C atom of acetylene while one of the Pd atoms is in the direct interaction with two C atoms, simultaneously in the TS1 and IM1 complexes via the two BCPs (No. 5 and 6 in TS1 and No. 3 and 4 in IM1). The increase of the value of $r$ for the BCP of Pd-H bond (BCP2, BCP1, and BCP1 in the R1, TS1, and IM1 complexes, respectively) shows that this bond becomes stronger due to the H transfer. Also, the strength of the Pd-N bond between the Pd atom and $g\text{-}C_3N_4$ becomes weaker in the IM1

(BCP No. 5; *r*=0.7159 a.u.) complex compared to the R1 complex (BCP No. 5; *r*=0.7015 a.u.) due to the decrease in its *r* value.

***IM1® TS2® IM2.*** Before the transfer of the second H atom in the structure of IM1 to the C atom of vinyl for forming IM3 (see Figure 7), a step is necessary (IM1®TS2®IM2). The second H atom is interacting with the Pd atom via the BCP1 in the structure of IM1. Notably, this H transfer becomes easier when the orientation of the complex above the g-$C_3N_4$ changes so that this Pd atom can directly interact with the N atoms of the substrate (see Figure 6; IM2). Due to this interaction, the IM2 complex is more stable than the IM1 complex and the orientation of the Pd-H bond is more suitable for the second H transfer to the C atom of vinyl compared to what is observed in the IM1. The bond angle of C-Pd-H in the structure of IM1 is 160.8° and reaches 83.9° in the structure of IM2 so that the distance between the second H atom and the C atom of vinyl decreases (see Figure 6). As seen, the orientation of the complex on the g-$C_3N_4$ changes so that the two Pd atoms are in direct interaction with the N atoms of g-$C_3N_4$. The strength of the H-Pd bond does not change due to this configuration change because of the small change of its *r* value. The calculated value of *r* of the H-Pd bond in the IM1 (BCP1) is 0.1484 a.u. and the corresponding value in the IM2 is 0.1502 a.u. (BCP5). Moreover, a decrease is seen in the bond length of the formed C-H bond in step 1 in the IM2 complex (2.36 Å) compared to that in the IM1 complex (2.60 Å) which shows that this bond is stronger. Therefore, the transfer of the second H atom from the Pd atom to the C atom in the IM2 needs less activation energy compared to that of this process in the IM1. A considerable decrease in the *r* values of the C-Pd interaction paths of the TS2 structure compared to those of the C-Pd interaction paths of the IM1 structure is seen. For example, the *r* of the BCPs No.3 and 4 (0.9617 and 0.9885 a.u, respectively), related to the simultaneous interaction of one Pd atom with two C atoms in the structure of IM1, reduces to 0.3508 and 0.4902 a.u., respectively in the structure of TS2 showing the decrease of the strength of these bonds (see Figure 6). Also, the arrangement of the interaction paths in the IM2 shows that each Pd atom is mainly interacting with one C atom unlike what is observed for the IM1 and TS2 structures in which one of the Pd atoms is in the direct interaction with two C atoms, simultaneously. One important point related to the TS2 structure is that the orientation of the complex on the g-$C_3N_4$ is so that its interaction with the substrate takes place mainly via the H atoms (see BCPs No.4, 7, and 8 in Figure 6). The imaginary vibrational mode of the TS2 is shown in Figure S3. As seen, the H atom which is interacting with the g-$C_3N_4$ via the BCPs No. 7 and 8, moves out of the substrate plane.

***IM2® TS3® IM3.*** Figure 7 shows the transfer of the second H atom from the Pd atom to the C atom of vinyl via the TS3 structure and form of the IM3. The comparison of the structure of TS3 with IM2 shows that the bond angle of C-Pd-H related to BCPs No. 2 and 5 in IM2 decreases in the TS3 structure (see BCPs No. 2 and 4). Comparison of the value of *r* of the BCP5 in the IM2 (0.1502 a.u.) with that of the corresponding BCP in the structure of TS3 (BCP4 ; *r*= 0.1341 a.u. ) shows that the decrease of the strength of the Pd-H bond due to the decrease of the C-Pd-H bond angle. The imaginary vibrational mode of the TS3 is shown in Figure S4. The displacement vector of the H atom shows its transfer from the Pd atom to the C atom. Notably, a BCP (*r*=0.5594 a.u.) is seen between two Pd atoms in the structure of IM3 showing the interaction of two Pd atoms with each other which is absent in the structure of IM2 and TS3.

***IM4® TS4® IM5.*** Figure 8 shows the first step of the hydrogenation of ethylene to form ethane via TS4. A new $H_2$ molecule is added to the IM3 for forming the IM4 so that the $H_2$ molecule is located near the Pd atoms to feasible the breaking of the $H_2$ bond. As seen in the figure, the dissociation of the $H_2$ molecule takes place in the TS4 structure so that one of the H atoms of $H_2$ is connected to one of the Pd atoms via the BCP2, and the other one is pulled toward the carbon atom of ethylene so that it is in the direct interaction with three atoms via the three BCPs (BCP4, BCP5, and BCP3), simultaneously. The imaginary vibrational frequency of the TS4 is shown in Figure S4. As seen, the displacement vector of one of the H atoms shows its tendency for forming the bond with the C atom of ethylene. The imaginary frequency of this vibrational mode and the barrier energy for this hydrogen transfer is 409*i* $cm^{-1}$ and 12.28 kcal/mol, respectively. The comparison of the structure of IM4 with TS4 shows the decrease of the Pd-Pd distance so that a new BCP appears between two Pd atoms in the IM4 structure. The strength of the Pd-Pd interaction in IM5 is lower than that in IM4 because of the decrease of the *r* of BCP3 from IM4 to IM5. Comparison of the *r* value of C-H bond in TS4 (BCP4 ; 0.1557 a.u.) with the corresponding value in IM5 (BCP1 ; 0.2384 a.u.) shows the complete formation of the new C-H bond in IM5 compared to TS4.

***IM5® TS5® P.*** Figure 9 shows the last step of the hydrogenation mechanism related to the second H transfer from the Pd atom to the C atom of $CH_3CH_2$ via the TS5 structure to form ethane. As seen, this H atom interacts with the Pd atom via the BCP5 ( *r*= 0.1960 a.u.) in the structure of IM5. Also, the increase of the number of BCPs between the Pd atom and g-$C_3N_4$ is seen in the TS5 structure (BCPs No. 3 and 4) compared to the IM5 structure (BCP No. 6) which helps to the hydrogen transfer by the weakening of the Pd-H bond as well as the presence of the BCP1 between the H and the C atom in this structure. Comparison of the calculated value of *r* of the BCP2 (0.1484 a.u.) in the structure of TS5 with that of BCP5 (0.1960 a.u.) in the structure of IM5 shows the decrease of the strength of the Pd-H interaction and confirms the H transfer from the Pd atom to C atom. The calculated value of vibrational frequency of the imaginary vibrational mode of TS5 (see Figure S4) related to the H transfer is 535*i* $cm^{-1}$ which is in agreement with the literature [39]. After the transfer of the last H atom to the $CH_3CH_2$ and the formation of ethane (structure P in Figure 9), one of the Pd atoms becomes close to the substrate so which creates a folding in the structure of g-$C_3N_4$.

A comparison has been made between the imaginary vibrational frequencies of the TSs of the hydrogenation of acetylene using the $Pd_2$/g-$C_3N_4$ catalyst with that reported in the literature [39] for $Pd_1$/g-$C_3N_4$ (see Table 2). As seen, the calculated vibrational frequencies for the R1®TS1®IM1, IM4®TS4®IM5, and IM5®TS5®P steps of our work are smaller than the value reported by Zhao et al. [39]. The value of the imaginary vibrational frequency of the TS of IM1®TS2®IM2 is nearly equal to that reported by Zhao et al. for the $Pd_1$/g-$C_3N_4$ catalyst. The imaginary frequency of the transition state of IM2®TS3®IM3 is greater than that reported for the $Pd_1$/g-$C_3N_4$ catalyst.

## Selectivity and reactivity

As previously mentioned, the effective performance of a heterogeneous catalyst in the hydrogenation of acetylene is the production of ethylene with a smaller value of activation energy compared to that of ethane production [39-40]. According to Figure 4, the activation energy for the first H transfer reaction (R1-TS1-IM1) is equal to 6.77 kcal/mol and it is smaller than the values reported in the literature for the other heterogeneous catalyst (see Table 3). Also, the comparison of the activation energy of the R1-TS1-IM1 step obtained in this work using the $Pd_2/g\text{-}C_3N_4$ catalyst (6.77 kcal/mol) with the corresponding value reported by Zhao et al. [39] using the $Pd_1/g\text{-}C_3N_4$ catalyst (21.53 kcal/mol) shows that the increase of the number of Pd atom has a considerable effect on the decrease of activation energy of this step.

The selectivity of a heterogeneous catalyst in the acetylene hydrogenation, for the production of ethylene, increases by the decrease of the activation energy of the ethylene production step compared to that of the ethane production step. The selectivity (D$E$) is considered as the difference between the hydrogenation barrier ($E_{hydrogenation}$) and desorption barrier ($E_{desorption}$) of ethylene [39-40]. The higher value of $\Delta E$ leads to the higher selectivity of the catalyst for ethylene production. The calculated value of $\Delta E$ obtained in this work is 21.9 kcal/mol (see Table3) which is more than that reported by Zhao et al. for the $Pd_1/g\text{-}C_3N_4$ catalyst. This shows that the increase in the number of Pd atoms of the catalyst is accompanied by the increase of the selectivity of the catalyst for ethylene production.

# Conclusion

In this work, a theoretical mechanistic study of the hydrogenation of acetylene on the $Pd_2/g\text{-}C_3N_4$ heterogeneous catalyst was performed using the DFT and QTAIM calculations. The selectivity of this catalyst for the ethylene production was compared with those of the other catalysts reported in the literature (Pd(111) [45], $Al_{13}CoO_4$ [46], AlPd [47], $Pd1/g\text{-}C_3N_4$ [39]). It was observed that the $Pd_2/g\text{-}C_3N_4$ has more selectivity and activity for ethylene production compared to the mentioned catalyst. Also, the results of this work show that the clustering of the Pd atoms on the $g\text{-}C_3N_4$ increases the selectivity and activity of the catalyst for the acetylene hydrogenation. This work provides strong insights for further research on the role of different palladium clusters deposited on graphitic carbon nitride material in acetylene hydrogenation.

# Declarations


## Acknowledgment

The authors thank Isfahan University of Technology (IUT) for its supports. The authors gratefully acknowledge the Shaikh Bahaie National High-Performance Computing Center (SBNHPCC) for providing a computing Facility.

## Funding

The authors thank Isfahan University of Technology (IUT) for its supports.

### The contribution of Authors

All authors conceived and designed the calculations; analyzed and interpreted the data; contributed materials, analysis tools, or data and software; and wrote the paper.

### Conflict of interest

The authors declare that they have no conflict of interest

### Availability of data and material

All data generated or analyzed during this study are included in this published article [and its supplementary information files].

### Code availability

N/A

# References


[1] Pradier C M, Mazina M, Berthier Y, Oudar J (1994) Hydrogenation of acetylene on palladium. J Mol Catal 89: 211-220.

[2] Sarkany A, Geszti O, Safran G (2008) Preparation of Pd shell–Au core/$SiO_2$ catalyst and catalytic activity for acetylene hydrogenation. Appl Catal A: Gen 350: 157–163.

[3] Wang P, Yang B Influence of surface strain on activity and selectivity of Pd-based catalysts for the hydrogenation of acetylene: A DFT study (2018) Chinese J Catal 39: 1493–1499.

[4] Lopez N, Vargas-Fuentes C (2012) Promoters in the hydrogenation of alkynes in mixtures: insights from density functional theory. Chem Commun 48: 1379–1391.

[5] Studt F, Abild-Pedersen F, Bligaard T, Sørensen R Z, Christensen C H, Norskov J K (2008) On the role of surface modifications of palladium catalysts in the selective hydrogenation of acetylene. Angew Chem Int Ed 47: 9299–9302.

[6] Vile G, Albani D, Nachtegaal M, Chen Z, Dontsova D, Antonietti M (2015) A stable single-site palladium catalyst for hydrogenations. Angew Chem 54: 11265.

[7] Huang X, Xia Y, Cao Y, Zheng X, Pan H, Zhu J (2017) Enhancing both selectivity and coking-resistance of a single-atom $Pd_1/C_3N_4$ catalyst for acetylene hydrogenation. Nano Res 10: 1302–1312.

[8] Kyriakou G, Boucher M B, Jewell A D, Lewis E A, Lawton T J, Baber A E (2012) Isolated metal atom geometries as a strategy for selective heterogeneous hydrogenations. Science 2012 335: 1209.

[9] Liu J, Bunes B R, Zang L, Wang C (2013) Supported single-atom catalysts: synthesis, characterization, properties, and applications. Environ Chem Lett 2017: 1–29.

[10] Kang L, Cheng B, Zhu M (2019) Pd/MCM-41 catalyst for acetylene hydrogenation to ethylene. R Soc Open Sci 6: 191155-191166.

[11] Panpranot J, Kontapakdee K, Praserthdam P (2006) Selective hydrogenation of acetylene in excess ethylene on micron-sized and nanocrystalline $TiO_2$ supported Pd catalysts. Appl Cat A Gen 314: 128–133.

[12] Panpranot J, Kontapakdee K, Praserthdam P (2006) Effect of $TiO_2$ crystalline phase composition on the physicochemical and catalytic properties of $Pd/TiO_2$ in selective acetylene hydrogenation. J Phys Chem B 110: 8019–8024.

[13] Meng L D, Wang G C (2014) A DFT + U study of acetylene selective hydrogenation over anatase supported $Pd_aAg_b$ (a + b = 4) cluster. Phys Chem Chem Phys 16: 17541-17551.

[14] Yang J, Cao L X, Wang G C (2012) Acetylene hydrogenation on anatase $TiO_2$ (101) supported $Pd_4$ cluster: oxygen deficiency effect. J Mol Model 18: 3329–3339.

[15] Ma L L, Lv C Q, Wang G C (2017) A DFT study and micro-kinetic analysis of acetylene selective hydrogenation on Pd-doped Cu (111) surfaces. Appl Surf Sci 410: 154–165.

[16] Yang J, Lv C Q, Guo Y, Wang G C (2012) A DFT+U study of acetylene selective hydrogenation on oxygen defective anatase (101) and rutile (110) $TiO_2$ supported $Pd_4$ cluster. J Chem Phys 136: 104107-104122.

[17] Li J N, Pu M, Ma C C, Tian Y, He J, Evans D J (2012) The effect of palladium clusters (Pdn, n = 2–8) on mechanisms of acetylene hydrogenation: A DFT study. J Mol Catal A: Chem 359: 14–20.

[18] Boyukata M, Belchior J C (2008) Molecular dynamics study of palladium clusters: size dependent analysis of structural stabilities and energetics of Pdn (n<40) via a lennard-jones type potential. Croatica Chem Act 81: 289-297.

[19] Moc J, Musaev D J, Morukama D (2003) Activation and adsorption of multiple $H_2$molecules on a $Pd_5$cluster: a density functional study. J Phys Chem A 107: 4929-4939.

[20] Zhou C, Yao S, Wu J, Forrey R C, Chen. L, Tachibana A, Chen H (2008) Hydrogen dissociative chemisorption and desorption on saturated sub nano palladium clusters (Pdn, n = 2–9). Phys Chem Chem Phys 10: 5445–5451.

[21] Cao Y, Sui Z, Zhu Y, Zhou X, Chen D (2017) Selective hydrogenation of acetylene over Pd-$In/Al_2O_3$catalyst: promotional effect of indium and composition-dependent performance. ACS Catal 7: 7835–7846.

[22] Albani D, Shahrokhi M, Chen Z, Mitchell S, Hauert R, Lopez N, Pérez-Ramírez J (2018) Selective ensembles in supported palladium sulfide nanoparticles for alkyne semi-hydrogenation. J Nat Commun 9: 2634-2644.

[23] Lopez N, Vargas-Fuentes C (2012) Promoters in the hydrogenation of alkynes in mixtures: insights from density functional theory. Chem Commun 48: 1379–1391.

[24] Volpe M A, Rodriguez P, Gigola C E (1999) Preparation of Pd–Pb/α-$Al_2O_3$ catalysts for selective hydrogenation using $PbBu_4$: the role of metal-support boundary atoms and the formation of a stable surface complex. Catal Lett 61: 27–32.

[25] Anderson J A, Mellor J, Wells R P K (2009) Pd catalyzed hexyne hydrogenation modified by Bi and by Pb. J Catal 261: 208–216.

[26] Kim S K, Lee L H, Ahn I K, Kim W J, Moon S H (2011) Performance of Cu-promoted Pd catalysts prepared by adding Cu using a surface redox method in acetylene hydrogenation. ApplCatalA Gen 401: 12–19.

[27] Gonzalez S, Neyman K M, Shaikhutdinov S, Freund H J, Illas F (2007) On the promoting role of Ag in selective hydrogenation reactions over Pd–Ag bimetallic catalysts: a theoretical study. J Phys Chem C 111: 6852–6856.

[28] Mei D, Neurock M, Smith C M (2009) Hydrogenation of acetylene–ethylene mixtures over Pd and Pd–Ag alloys: first-principle based kinetic Monte Carlo simulations. J Catal 268: 181–195.

[29] Sheth P A, Neurock M, Smith C M (2009) First-principles analysis of the effects of alloying Pd with Ag for the catalytic hydrogenation of acetylene–ethylene mixtures. J Phys Chem B 109: 12449–12466.

[30] Kumar N, Ghosh P (2016) Selectivity and reactivity of Pd-rich Pd-Ga surfaces toward selective hydrogenation of acetylene: interplay of surface roughness and ensemble effect. J Phys Chem C 120: 28654–28663.

[31] Osswald J, Giedigkeit R, Jentoft R E, Armbrüster M, Girgsdies F, Kovnir K (2008) Palladium–gallium intermetallic compounds for the selective hydrogenation of acetylene. Part I. Preparation and structural investigation under reaction conditions. J Catal 258: 210–218.

[32] Zhou H, Yang X, Wang A, Miao S, Liu X, Pan X (2016) Pd/ZnO catalysts with different origins for high chemoselectivity in acetylene semi-hydrogenation. Chin J Catal 37: 692–699.

[33] Gulyaeva Y K, Kaichev V V, Zaikovskii V I, Kovalyov E V, Suknev A P, Balzhinimaev B S (2015) Selective hydrogenation of acetylene over novel Pd/fiberglass catalysts. Catal Today 245: 139–146.

[34] Yan H, Cheng H, Yi H, Lin Y, Yao T, Wang T (2015) Single-atom $Pd_1$/Graphene catalyst achieved by atomic layer deposition: remarkable performance in selective hydrogenation of 1,3-butadiene. J Am Chem

Soc 137: 10484–10487.

[35] Komhom S, Mekasuwandumrong O, Praserthdam P, Panpranot J (2008) Improvement of $Pd/Al_2O_3$ catalyst performance in selective acetylene hydrogenation using mixed phases $Al_2O_3$ support. Catal Commun 10: 86–91.

[36] Hosseini S M, Ghiaci M, Kulinich S A, Wunderlich W, Farrokhpour H, Saraji M, Shahvar A (2018) Au-Pd@g-$C_3N_4$ as an efficient photocatalyst for visible-light oxidation of benzene to phenol: experimental and mechanistic study. J Phys Chem C 122: 27477–27485.

[37] Shahzeydi A, Ghiaci M, Farrokhpour H, Shahvar A, Sun M, Saraji M (2019) Facile and green synthesis of copper nanoparticles loaded on the amorphous carbon nitride for the oxidation of cyclohexane. Chem Eng J 370: 1310-1321.

[38] Nilforoushan S, Ghiaci M, Hosseini S M, Laurent S, Muller R N (2019) Selective liquid phase oxidation of ethyl benzene to acetophenone by palladium nanoparticles immobilized on a g-$C_3N_4$–rGO composite as a recyclable catalyst. New J Chem 46: 6921-6931.

[39] Zhao Y, Zhu M, Kang L (2018) The DFT study of single-atom $Pd_1/g\text{-}C_3N_4$catalyst for selective acetylene hydrogenation reaction. Cattal Lett 148: 2992–3002.

[40] Kang L, Zhu M, Zhao Y (2019) A DFT study of acetylene hydrogenation catalyzed by S-doped $Pd_1/g\text{-}C_3N_4$. Catalysts 9: 887-899.

[41] Hosseini S M, Ghiaci M, Farrokhpour H (2019) The adsorption of small size Pd clusters on a g-$C_3N_4$ quantum dot: DFT and TD-DFT study. Mater Res Express 6: 105079-105093.

[42] Singh N B, Sarkar U (2014) Structure, vibrational, and optical properties of platinum cluster: a density functional theory approach. J Mol Model 20: 2537–2548.

[43] Lu T, Chen F (2012) Multiwfn: a multifunctional wavefunction analyzer. J Comput Chem 33: 580–592.

[44] Frisch M J (2013) Gaussian 09, Revision D.01, Wallingford, CT: Gaussian, Inc.

[45] Mei D, Sheth P A, Neurock M, Smith C M (2006) First-principles based kinetic Monte Carlo simulation of the selective hydrogenation of acetylene over Pd (111). J Catal 242: 1–15.

[46] Krajci M, Hafner J (2011) Complex intermetallic compounds as selective hydrogenation catalysts—a case study for the (100) surface of $Al_{13}Co_4$. J Catal 278: 200–207.

[47] Krajci M, Hafner J (2012) Intermetallic compound AlPd as a selective hydrogenation catalyst: a DFT study. J Phys Chem C 116: 6307–6319.

# Table

**Table 1. The energies of the HOMO and LUMO of $C_2H_2$, $H_2$, g-$C_3N_4$, $Pd_2$/g-$C_3N_4$, and $Pd_2$/g-$C_3N_4$·$C_2H_2$ compounds and their corresponding energy gaps**

| | HOMO | LUMO | $\Delta E_g$ |
|---|---|---|---|
| $H_2$ | -11.74 (eV) | 1.84 | -9.89 |
| $C_2H_2$ | -8.25 | 0.45 | -7.79 |
| g-$C_3N_4$ | -6.53 | -2.62 | -3.90 |
| $Pd_2$/g-$C_3N_4$ | -4.71 | -2.71 | -2.00 |
| $Pd_2$/g-$C_3N_4$·$C_2H_2$ | -4.09 | -2.67 | -1.41 |

**Table 2. The imaginary frequencies of the transition states (TSs) involved in the different steps of the acetylene hydrogenation mechanism taken from Zhao's group work [39] for the Pd1/g-$C_3N_4$ with those obtained in this work.**

| Imaginary Frequency ($cm^{-1}$) | | | | | Catalyst |
|---|---|---|---|---|---|
| IM5-TS5-P | IM4-TS4-IM5 | IM2-TS3-IM3 | IM1-TS2-IM2 | R1-TS1-IM1 | |
| 760.9*i* | 685.08*i* | 641.95*i* | 724.3*i* | 750.62*i* | $Pd_1$/g-$C_3N_4$ |
| 535*i* | 409*i* | 711*i* | 723.1*i* | 476*i* | $Pd_2$/g-$C_3N_4$ |

**Table 3. Comparison of the ctivation energies for the first hydrogen transfer to the acetylene and ethylene reported in literature with those obtained in this work.**

| Reference | Selectivity (ΔE) | Energy barrier (kcal/mol) | | Catalyst |
|---|---|---|---|---|
| | | $C_2H_4 + H_2 \rightarrow C_2H_6$ | $C_2H_2 + H_2 \rightarrow C_2H_4$ | |
| 45 | 2.45 | 17.61 | 18.1 | Pd(111) |
| 46 | 6.34 | 19.57 | 15.41 | $Al_{13}CoO_4$ |
| 47 | 11.25 | 13.7 | 18.59 | AlPd |
| 39 | 15.4 | 38.88 | 21.53 | $Pd_1$/g-$C_3N_4$ |
| This Study | 21.9 | 12.28 | 6.77 | $Pd_2$/g-$C_3N_4$ |

# Figures

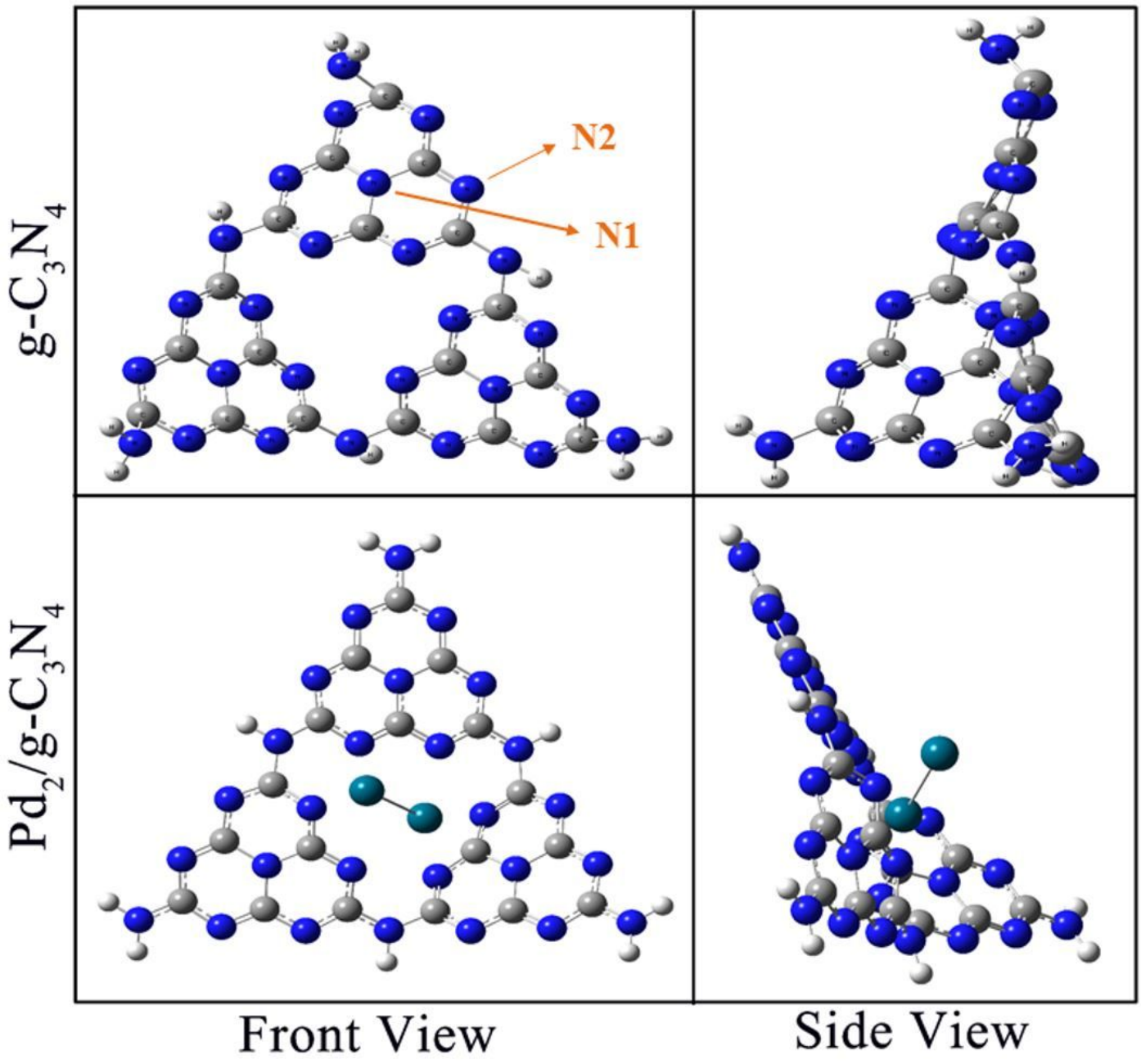


**Figure 1**

The optimized structures of the g-C3N4 quantum dot and the Pd2/g-C3N4 catalyst shown in two different views.

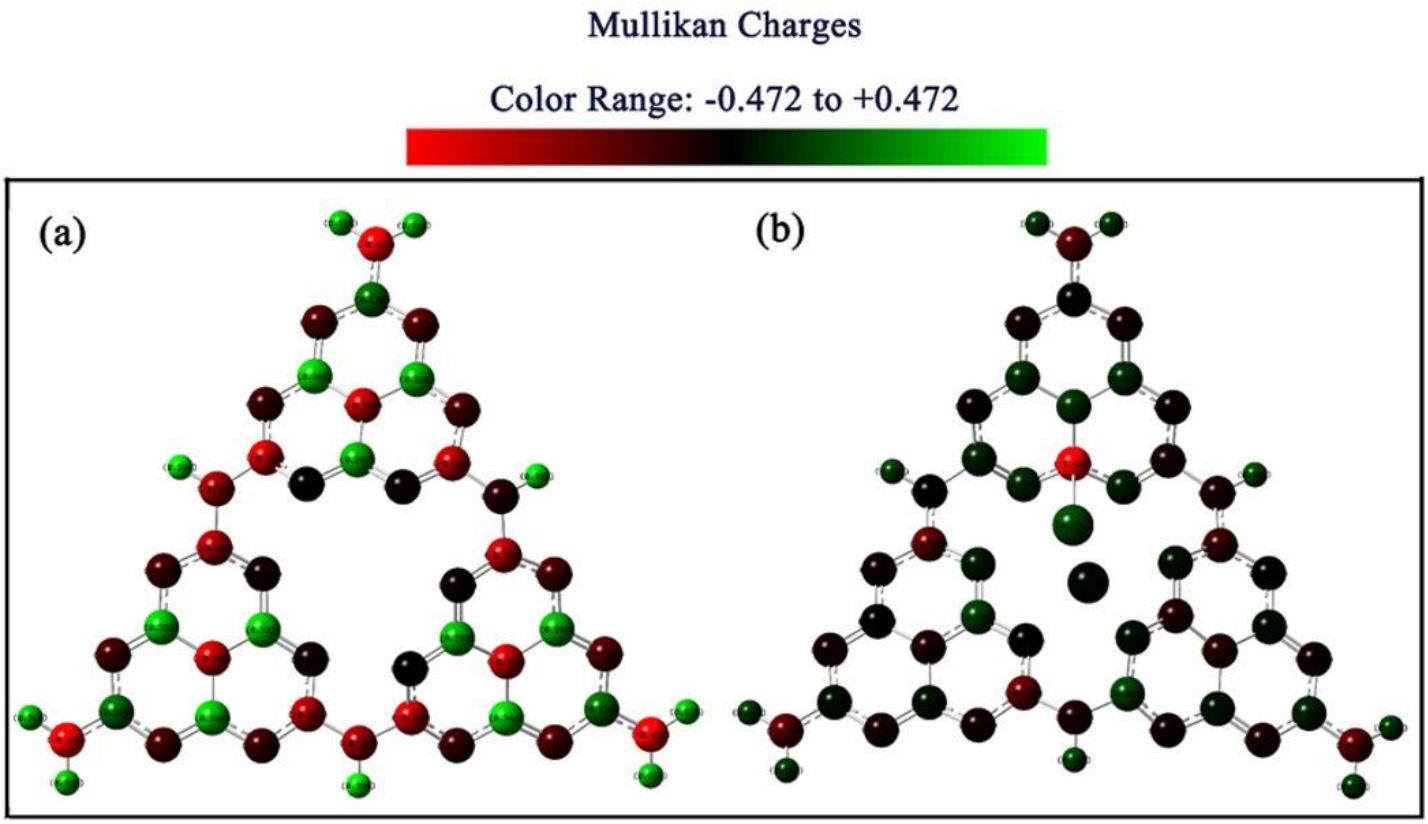


## Figure 2

Mulliken partial atomic charges distribution of (a) g-C3N4 quantum dot and (b) Pd2/g-C3N4 complex.

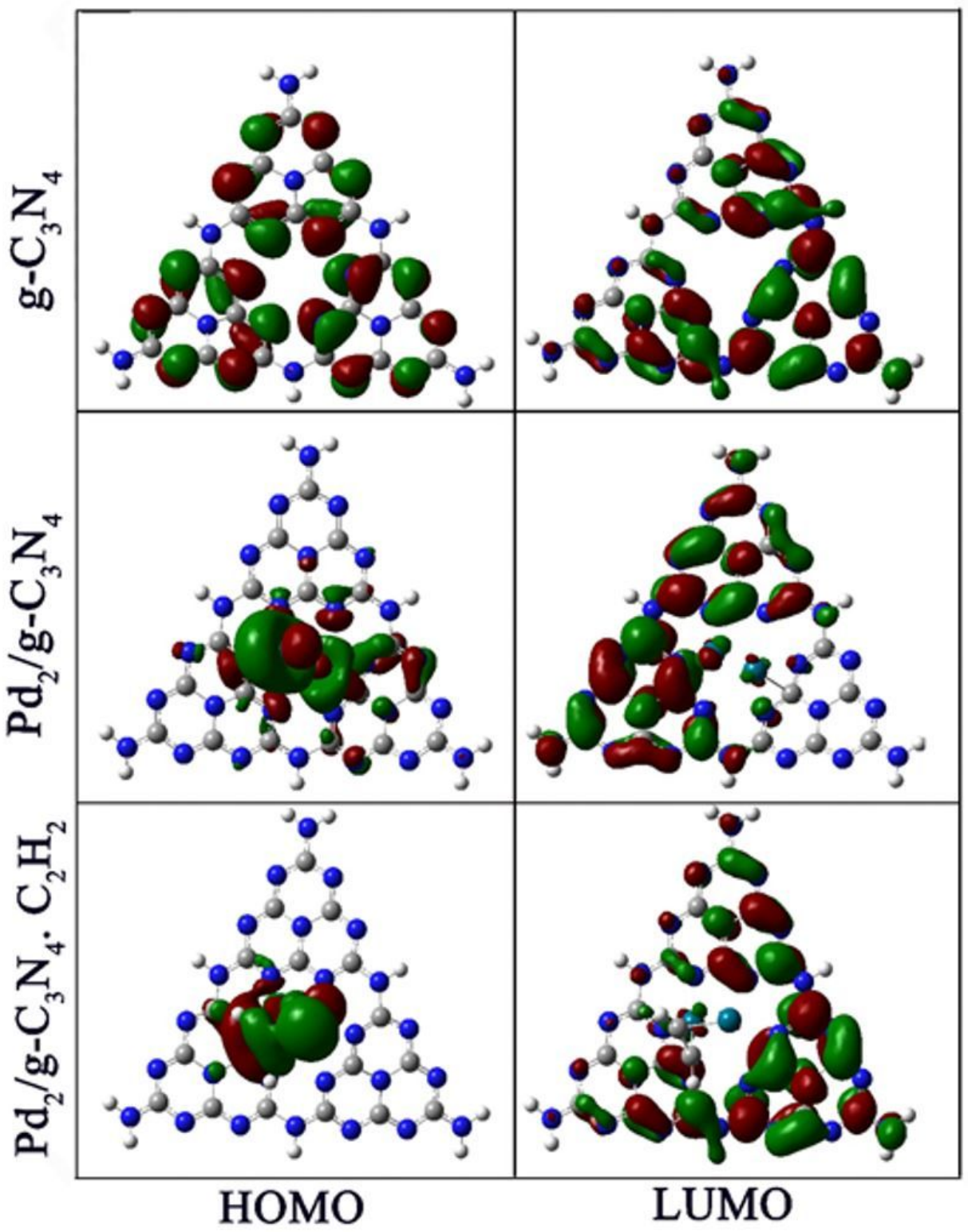


**Figure 3**

Frontier molecular orbitals of the g-C3N4, Pd2/g-C3N4, and C2H2.Pd2/g-C3N4 structures

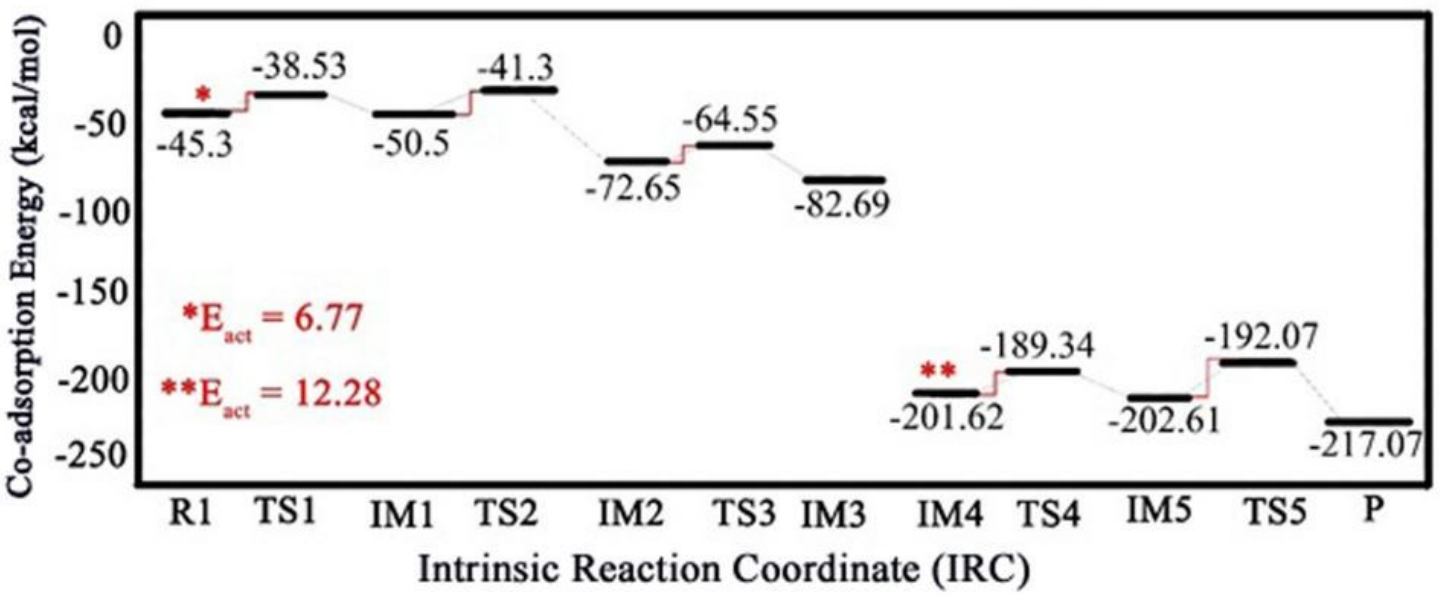


**Figure 4**

Energy diagram for the acetylene hydrogenation over the Pd2/g-C3N4 catalyst

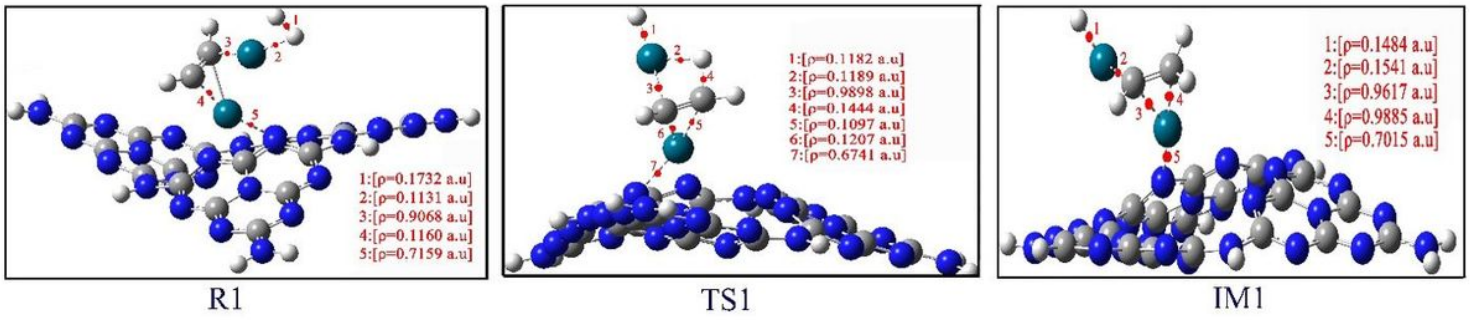


**Figure 5**

The optimized structure of the R1, TS1, and IM1 of the first step of hydrogenation of acetylene on the Pd2/g-C3N4 catalyst. The red points show the position of the bond critical points (BCPs) obtained from the QTAIM calculations. The value of electron density (□) for each BCP has been given.

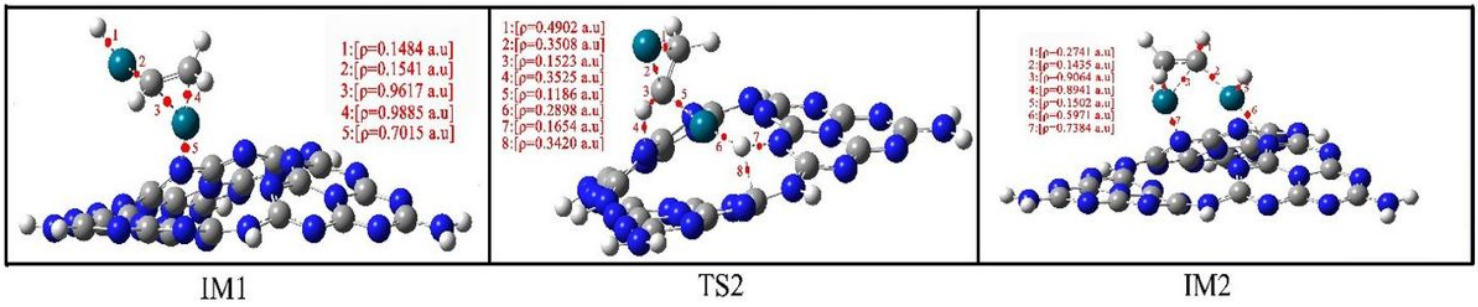


**Figure 6**

The optimized structure of the IM1, TS2, and IM2 of the second step of hydrogenation of acetylene on the Pd2/g-C3N4 catalyst. The red points show the position of the bond critical points (BCPs) obtained from the QTAIM calculations. The value of electron density (ρ) for each BCP has been given.

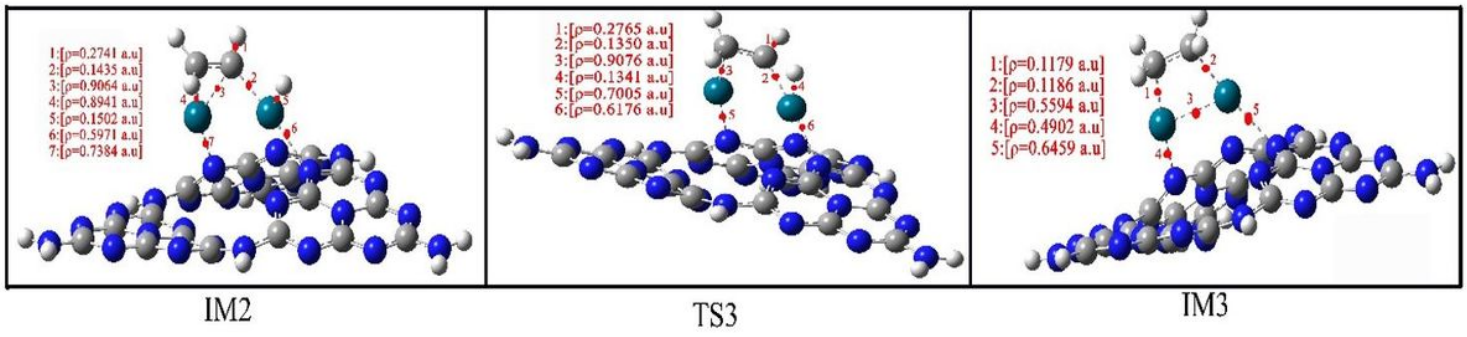


**Figure 7**

The optimized structure of the IM2, TS3, and IM3 of the third step of hydrogenation of acetylene on the Pd2/g-C3N4 catalyst. The red points show the position of the bond critical points (BCPs) obtained from the QTAIM calculations. The value of electron density (ρ) for each BCP has been given.

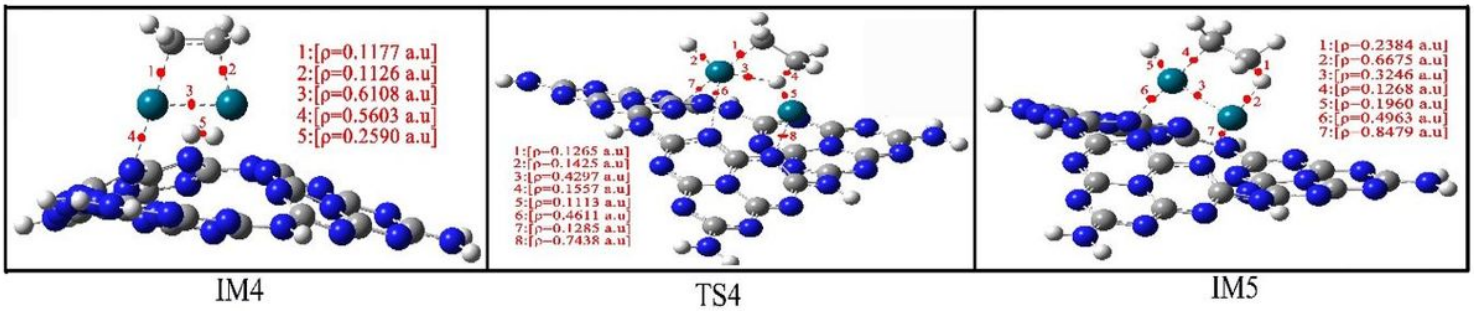


**Figure 8**

The optimized structure of the IM4, TS4, and IM5 of the first step of hydrogenation of ethylene on the Pd2/g-C3N4 catalyst. The red points show the position of the bond critical points (BCPs) obtained from the QTAIM calculations. The value of electron density (ρ) for each BCP has been given.

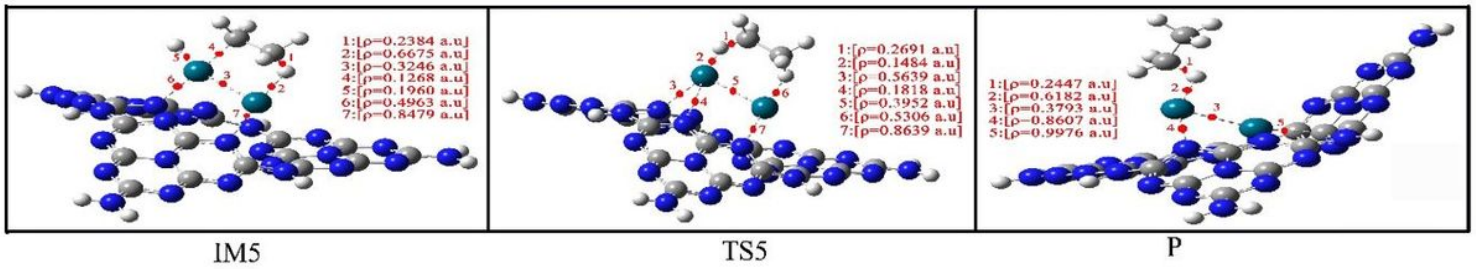


**Figure 9**

The optimized structure of the IM5, TS5, and P of the second step of hydrogenation of ethylene on the Pd2/g-C3N4 catalyst. The red points show the position of the bond critical points (BCPs) obtained from the QTAIM calculations. The value of electron density (ρ) for each BCP has been given.

# Supplementary Files

This is a list of supplementary files associated with this preprint. Click to download.

- SupportingInformation22.docx